Virtual Raman *KLL* radiative Auger process

Yeon Deog Koo and K. Das Gupta*
Department of Physics, Texas Tech University, P. O. Box 4180, Lubbock, Texas 79409
(Received 26 February 1990)

By x-ray bombardment of metal single crystals, x rays of *KLL* radiative Auger electrons are observed on the low-energy side of the $K\alpha$ lines. Unlike the usual radiative Auger process where x-ray continua result, we find x rays in the form of sharp lines that originate from a hitherto unobserved virtual Raman process. To our surprise this is the dominant radiative Auger process in the investigated single crystals.

I. INTRODUCTION

In 1969, Åberg and Utriainen[1] observed a structure including several maxima on the low-energy side of the $K\alpha$ doublet in Mg, Si, and S. The maxima were interpreted as heads of radiation continua corresponding to the ejection of L electrons with kinetic energies increasing from zero at the heads of the continua. Jamison *et al.*[2] observed a similar result by heavy-ion bombardment. The x rays resulting from the one-photon two-electron rearrangement for Mg, Al, and Si by heavy-ion bombardment originated from radiative Auger electron (RAE) and radiative electron rearrangement (RER). Bonnet *et al.*[3] showed evidence of RAE in the Ar L x rays spectrum produced by electron impact. The relative intensity[4–7] of RAE and $K\alpha$[4–7] has been studied. Åberg[4] has shown that the simultaneous emission of an x-ray photon and electron can occur as a consequence of the change in the average potential acting on the electron when the x-ray hole is moving from an inner to an outer shell and as a consequence of interaction between single- and double-hole configuration in the final state. The relative probabilities of *KLL* transition were calculated for some elements by Åberg. Kostroun and Baptista[5] calculated the spectral distribution of emitted photons following *KMM* RAE transitions in the free argon atom. Recently, Das Gupta[8] observed a sharp x-ray line of *KLL* RAE in a Ni single crystal excited by a tungsten x-ray tube, indicative of the existence of a radiative Auger process that differs from the one that gives rise to an x-ray continuum. It is a Raman-like process, the study of which is reported in this paper. We point out that previous work on the radiative Auger process was done generally on polycrystalline samples, whereas our studies involve single-crystal samples. A single crystal has the advantage that the x rays of RAE are more readily detectable via Bragg channeling.

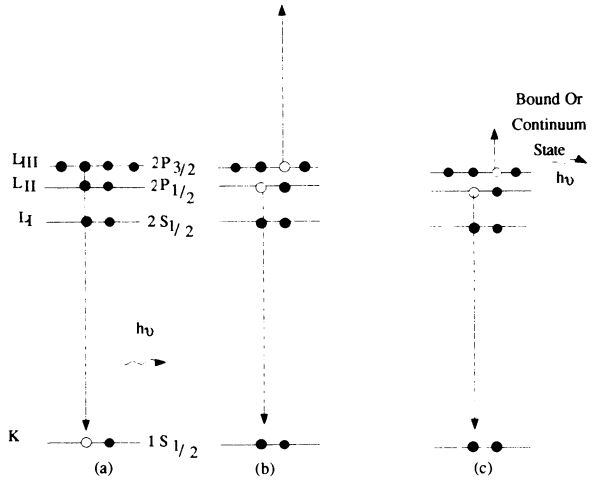

FIG. 1. (a) $K\alpha$ x-ray emission, (b) nonradiative Auger process, and (c) radiative Auger process.

II. VIRTUAL RAMAN *KLL* RADIATIVE AUGER PROCESS

When an electron is knocked out of the K shell of an atom by x-ray (or electron) bombardment, the reorgani-

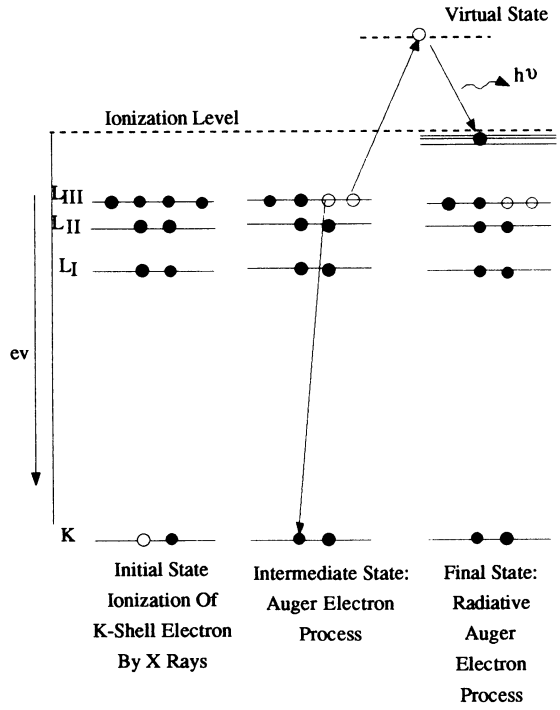

FIG. 2. Virtual Raman RAE process. The Auger electron is bound to an unoccupied optical level close to the Fermi surface and radiates an x-ray photon.

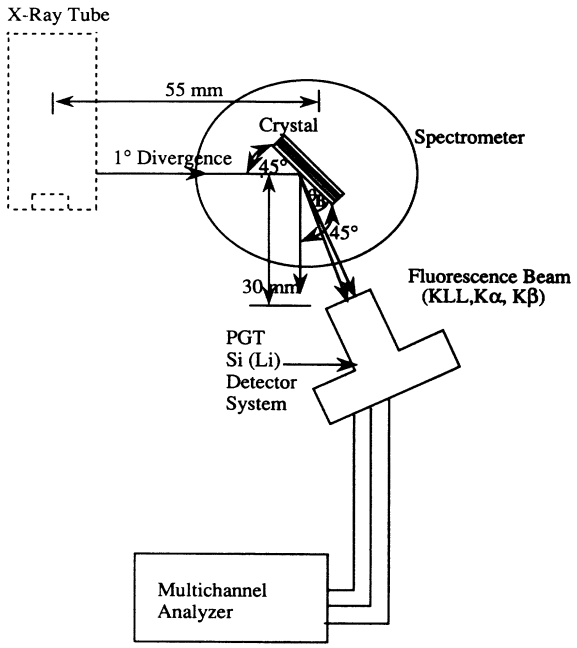

FIG. 3. Experimental system. The monocrystals are fixed at 45° and the Si(Li) detector is set between the Bragg angles of $K\alpha$ and KLL to avoid the reflected beam of incident x rays.

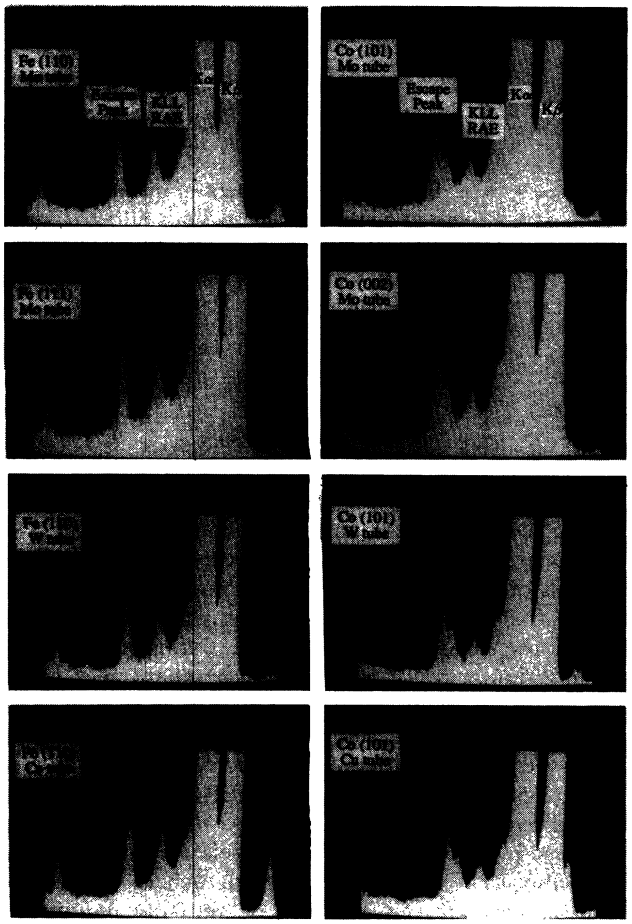

FIG. 4. KLL RAE and other fluorescence of Fe and Co crystals. Photographs of multichannel analyzer display screen show x-ray peaks of $K\beta$, $K\alpha$, KLL RAE, and Si escape peak of $K\alpha$. The left photographs are for Fe(110) and (111) single crystals and the right ones for Co(101) and (002) single crystals with Mo, W, and Cu target x-ray tubes used.

zation of the atom can proceed by several mechanisms. For instance, an electron can jump from the L or M shell to fill the K vacancy. This jump is accompanied by the emission of a $K\alpha$ or $K\beta$ photon, respectively, as seen in Fig. 1(a), and corresponds to x-ray fluorescence. The reorganization can also proceed by jump of an L or M electron to the K vacancy and the simultaneous ejection of an L or M electron from the atom. This is the nonradiative Auger process depicted in Fig. 1(b). If the electron ejection is accompanied by photon emission, the Auger process is radiative, as depicted in Fig. 1(c).

If the relaxation occurs through an L_i electron accompanied by the emission of another L_j electron, the transition is termed KL_iL_j RAE; if it occurs through an M_i electron accompanied by the emission of another M_j electron, the transition is termed KM_iM_j. The KL_iL_j RAE is less energetic than the corresponding $K\alpha$ emission line and its energy is given by

$$h\nu = E(KL_iL_j) - E_{\text{kin}}(L_j) ,$$

where $E_{kin}(L_j)$ is the kinetic energy of the emitted electron and $E(KL_iL_j)$ is the energy of the KL_iL_j Auger electron. The kinetic energy of the emitted electron varies from zero to $E(KL_iL_j)$ and the photon $h\nu$ has continuous energy values with a maximum value equal to $E(KL_iL_j)$ for $E_{\text{kin}}(L_j)=0$; this maximum value corresponds to the most probable transition.

The earlier observation by Das Gupta of an x-ray line,

TABLE I. Comparison of the measured energies of KLL RAE with KL_1L_2 and KL_2L_3 energies, which correspond to the most probable Auger states. ESCA denotes electron spectroscopy for chemical analysis.

		Measured energies (eV) (Expt. results)			ESCA E (eV) (Calc. values)	
		Mo tube	W tube	Cu tube	KL_1L_2	KL_2L_3
Fe	(111)	5440			5580	5622
	(110)	5436	5436	5435	5514	
Co	(002)	5933			5923	6075
	(101)	5939	5950	5928	5957	
Ni	(200)	6422			6384	6542
	(111)	6422	6420	6420	6419	
Cu	(111)	7054			6861	7030
	(200)	7054	7058	7058	6896	

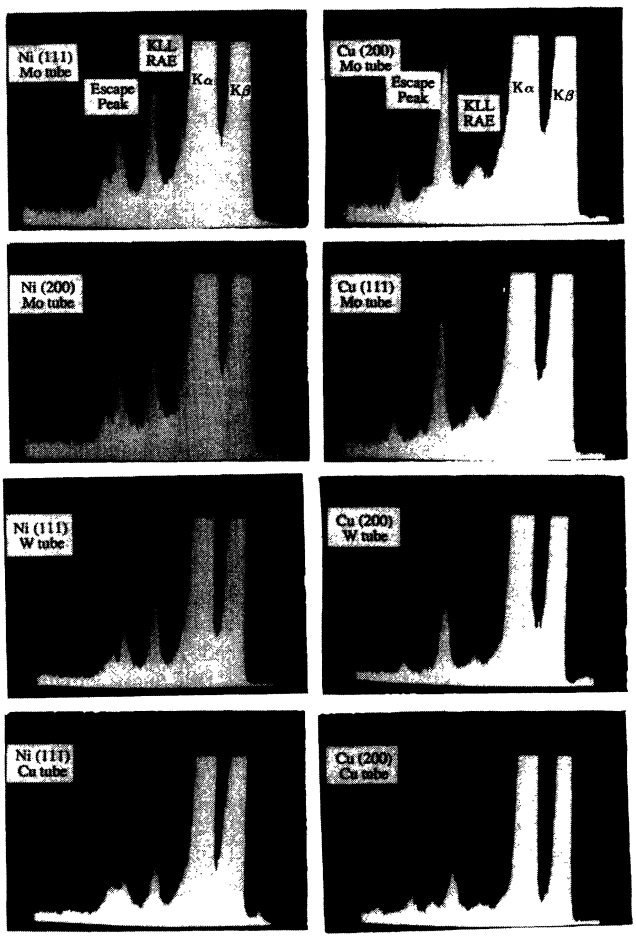

FIG. 5. *KLL* RAE and other fluorescence of Ni and Cu single crystals. Photographs show x-ray peaks of $K\beta$, $K\alpha$, *KLL* RAE, and Si escape peak of $K\alpha$. The left photographs are for Ni(111) and (200) single crystals and the right ones for Cu (200) and (111) single crystals with Mo, W, and Cu target x-ray tubes used.

rather than a continuum, in a Ni single crystal implies the occurrence of another Auger process. It is depicted in Fig. 2. In the intermediate state, it is assumed that the characteristic x ray is produced when an electron in a high-energy shell drops down to fill the K hole and is absorbed by the emitted Auger electron by inelastic scattering. The x ray absorbed by the Auger electron is a virtual photon. Therefore we term the process a virtual Raman process.

III. EXPERIMENTAL DETAIL

The experimental apparatus consists of x ray tube, collimator, spectrometer with crystal, and detector system (Fig. 3). The crystals under investigation were Fe(110), Fe(111), Co(101), Co(002), Ni(111), Ni(200), Cu(200), and Cu(111) single crystals cut parallel to these faces. The crystals were excited by molybdenum, tungsten, or copper target radiation.

The x-ray tubes were operated to obtain 5% dead time of the detector system. The best results were obtained at 30 kV, 1 mA for the Mo tube, 20 kV, 1 mA for the W tube, and 18 kV, 1 mA for the Cu tube for efficient ionization of K-shell electrons. The collimator attached to the x-ray tubes produced 1° angular divergence of the beam.

A precision x-ray spectrometer with 1-min vernier scale holds the crystal at its axis of rotation. The axes of the single crystals are aligned accurately parallel to the rotational axis of the spectrometer. The solid-state detector Si(Li) is cooled by liquid nitrogen. Its energy resolution is 150 eV. The multichannel analyzer (MCA) display of the detector system records counts for the observed spectral lines. The energy calibration is done with ^{55}Fe and ^{109}Cd radioisotopes at 5898 and 22 163 eV. The energy calibration error is within ± 10 eV.

The crystals are set at 45° with respect to the collimated target radiation. The detector is set between $K\alpha$ and *KLL* RAE Bragg angles from the crystal surface. The thickness of the beryllium window of the detector is 5 mm and the detector is set at a distance of 30 mm from the rotational axis of the crystal, from which the solid angle of the detector is calculated to be 10°. The detector receives $K\alpha$, $K\beta$, and *KLL* RAE x rays simultaneously because the differences of these Bragg angles are within 6°. Because all of the Bragg angles for *KLL* and $K\alpha$ of Fe, Co, Ni, and Cu are less than 34°, the detector absorbs only *KLL* and K fluorescence lines and misses the bremsstrahlung that is Bragg reflected at 45°.

TABLE II. Relative intensities of *KLL* x rays, $K\beta$, and Si $K\alpha$ escape peaks to $K\alpha$.

		Fe		Co		Ni		Cu	
Ratio (%)	Tube	(111)	(110)	(002)	(101)	(200)	(111)	(111)	(200)
$I(KLL)/I(K\alpha)$	Mo tube	0.35	0.38	0.22	0.24	0.43	0.44	0.18	0.16
	W tube		0.38		0.25		0.49		0.21
	Cu tube		0.43		0.25		0.67		0.43
$I(K\beta)/I(K\alpha)$	Mo tube	14.7	15.3	15.1	15.4	15.2	14.9	15.5	15.2
	W tube		14.5		14.8		15.1		15.1
	Cu tube		14.6		14.2		14.6		14.5
I(Si escape peak)$/I(K\alpha)$	Mo tube	0.38	0.44	0.035	0.37	0.34	0.30	0.55	0.49
	W tube		0.46		0.42		0.29		0.57
	Cu tube		0.42		0.42		0.47		0.74

IV. EXPERIMENTAL RESULTS AND ANALYSIS

Figures 4 and 5 show the experimental results displayed on the MCA for Fe(110), Fe(111), Co(101), Co(002), Ni(111), Ni(200), Cu(111), and Cu(200) single crystals when Mo, W, and Cu target x-ray tubes are used to excite atoms in the crystals. The photographic picture for each crystal shows the x-ray peaks of $K\beta$, $K\alpha$, KLL, RAE, and the Si escape peak of $K\alpha$ from right to left. The MCA cursor position in the figures is on the KLL RAE lines. The Si escape peak originates from the excitation of Si atoms by the incident x rays, producing Si $K\alpha$ radiation at 1740 eV. The energy of the Si escape peak is 1740 eV less than the $K\alpha$ energy.

A. Energies of observed peaks of *KLL* RAE

According to previous theories[4–7] the MCA display should reveal x-ray continuum with a sharp edge at the limit when the kinetic energy of the Auger electron is zero. Our displays show that the RAE x rays form sharp peaks instead. This agrees with the assumption of a virtual Raman RAE process.

Table I shows the measured peak x-ray energies of the KLL RAE and the kinetic energies of the most probable Auger state[9] from electron spectroscopy for chemical analysis (ESCA) tables.[10] The peak energies of the observed lines do not change when different x-ray targets are used in exciting the crystals. Chen and Crasemann[9] calculated the KLL Auger transition probabilities. They predicted that the most probable states of KLL Auger electron for atomic numbers 26 to 29 are KL_2L_3, and KL_1L_2 as the next most probable state. As Table I shows, the detected values are closer to $KL_1L_{2,3}$ energies for Fe, Co, Ni, and KL_2L_3 for Cu than other Auger-electron states.

B. Intensities of observed *KLL* RAE

Table II shows the measured intensity ratios $I(KLL$ x-ray lines$)/I(K\alpha)$. Additionally, the $I(K\beta)/I(K\alpha)$ and I(Si escape peak$)/I(K\alpha)$ ratios are measured. The intensity ratios of the KLL RAE and $K\alpha$ are meaningful because they are competing decay branches of the same initial state which has one hole produced in the K shell by x-ray bombardment.

$I(K\beta)/I(K\alpha)$ intensity ratios were 14–15 % in agreement with Scofield's theoretical values[11] and the experimental values of Campbell *et al.*[12] Similarly, the values of I(Si escape peak$)/I(K\alpha)$ were in the range 0.3–0.57 % (Table II). These values agree with Russ's results.[13]

Our experimental results reveal that the intensity ratio of the $KLL/K\alpha$ are below 0.5% for Fe, Co, Ni, and Cu single crystals when excited by W, Mo, and Cu target radiation. The background intensity at the KLL energy is approximately 30% of the measured intensities of the peaks (Fig. 4). After its subtraction, the $I(KLL)/I(K\alpha)$ ratios are around 0.25%. These intensity ratios are close to Scofield's theoretical values,[11] which represent the percentage rates of production of KLL Auger electrons relative to the transition rate of $K\alpha$ lines. He predicted that the percentage ratio for iron is 0.28%. The agreement with the theoretical values indicates that the virtual Raman KLL RAE process is the dominant one in the investigated samples, a surprising result to us.

ACKNOWLEDGMENTS

This work was supported by the Texas Advanced Technology Program, Grant No. 1342.

*Author to whom correspondence should be addressed.

[1]T. Åberg and J. Utriainen, Phys. Rev. Lett. **22**, 1346 (1969).
[2]K. A. Jamison *et al.*, Phys. Rev. A **14**, 937 (1976).
[3]J-J. Bonnet *et al.*, J. Phys. B **13**, L187 (1980).
[4]T. Åberg, Phys. Rev. A **4**, 1735 (1971).
[5]V. O. Kostroun and G. B. Baptista, Phys. Rev. A **14**, 363 (1976).
[6]E. Marageter *et al.*, X-Ray Spectroscopy **13**, 78 (1984).
[7]G. Presser, Phys. Lett. **56A**, 273 (1976).
[8]K. Das Gupta (unpublished).
[9]M. H. Chen and B. Crasemann, Phys. Rev. A **8**, 7 (1973).
[10]K. Siegbahn *et al.*, *ESCA: Atomic, Molecular and Solid State Structure Studied by Means of Electron Spectroscopy* (Nova Acta Regiae Societatis Scientiarum Upsaliensis, Uppsala, Sweden, 1967), Ser. IV, Vol. 20, pp. 235–236.
[11]J. H. Scofield, Phys. Rev. A **9**, 1041 (1974).
[12]J. L. Campbell *et al.*, Phys. Rev. A **33**, 2410 (1986).
[13]J. C. Russ, Adv. X-Ray Anal. **19**, 161 (1975).

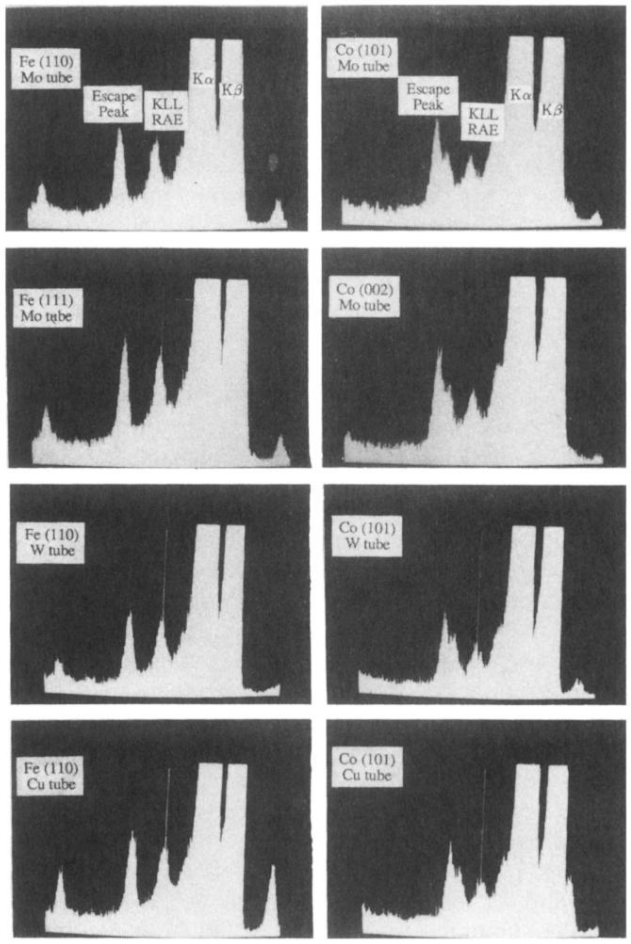

FIG. 4. *KLL* RAE and other fluorescence of Fe and Co crystals. Photographs of multichannel analyzer display screen show x-ray peaks of $K\beta$, $K\alpha$, *KLL* RAE, and Si escape peak of $K\alpha$. The left photographs are for Fe(110) and (111) single crystals and the right ones for Co(101) and (002) single crystals with Mo, W, and Cu target x-ray tubes used.

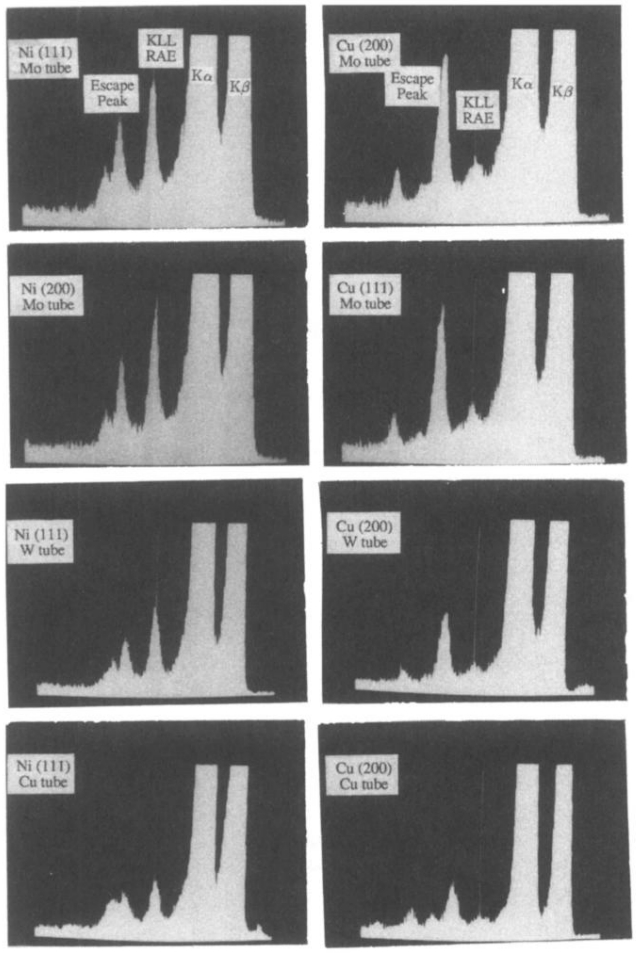

FIG. 5. *KLL* RAE and other fluorescence of Ni and Cu single crystals. Photographs show x-ray peaks of $K\beta$, $K\alpha$, *KLL* RAE, and Si escape peak of $K\alpha$. The left photographs are for Ni(111) and (200) single crystals and the right ones for Cu (200) and (111) single crystals with Mo, W, and Cu target x-ray tubes used.